Targeting the αv integrin/TGF-β axis improves natural killer cell function against glioblastoma stem cells

Hila Shaim,[1,2] Mayra Shanley,[1] Rafet Basar,[1] May Daher,[1] Joy Gumin,[3] Daniel B. Zamler,[4] Nadima Uprety,[1] Fang Wang,[5] Yuefan Huang,[5] Konrad Gabrusiewicz,[3] Qi Miao,[5] Jinzhuang Dou,[5] Abdullah Alsuliman,[1] Lucila N. Kerbauy,[1] Sunil Acharya,[1] Vakul Mohanty,[5] Mayela Mendt,[1] Sufang Li,[1] JunJun Lu,[1] Jun Wei,[3] Natalie W. Fowlkes,[6] Elif Gokdemir,[1] Emily L. Ensley,[1] Mecit Kaplan,[1] Cynthia Kassab,[3] Li Li,[1] Gonca Ozcan,[1] Pinaki P. Banerjee,[1] Yifei Shen,[5] April L. Gilbert,[1] Corry M. Jones,[1] Mustafa Bdiwi,[1] Ana K. Nunez-Cortes,[1] Enli Liu,[1] Jun Yu,[3] Nobuhiko Imahashi,[1] Luis Muniz-Feliciano,[1] Ye Li,[1] Jian Hu,[7] Giulio Draetta,[4] David Marin,[1] Dihua Yu,[8] Stephan Mielke,[2,9] Matthias Eyrich,[10] Richard E. Champlin,[1] Ken Chen,[5] Frederick F. Lang,[3] Elizabeth J. Shpall,[1] Amy B. Heimberger,[3] and Katayoun Rezvani[1]

[1]Department of Stem Cell Transplantation and Cellular Therapy, The University of Texas MD Anderson Cancer Center, Houston, Texas, USA. [2]Department of Internal Medicine II, University Medical Center Würzburg, Würzburg, Germany. [3]Department of Neurosurgery, [4]Department of Genomic Medicine, [5]Department of Bioinformatics and Computational Biology, [6]Department of Veterinary Medicine and Surgery, [7]Department of Cancer Biology, and [8]Department of Molecular and Cellular Oncology, The University of Texas MD Anderson Cancer Center, Houston, Texas, USA. [9]Department of Hematology, Karolinska Institute, Stockholm, Sweden. [10]Department of Pediatric Hematology, Oncology and Stem Cell Transplantation, University Medical Center Würzburg, Würzburg, Germany.

Glioblastoma multiforme (GBM), the most aggressive brain cancer, recurs because glioblastoma stem cells (GSCs) are resistant to all standard therapies. We showed that GSCs, but not normal astrocytes, are sensitive to lysis by healthy allogeneic natural killer (NK) cells in vitro. Mass cytometry and single-cell RNA sequencing of primary tumor samples revealed that GBM tumor–infiltrating NK cells acquired an altered phenotype associated with impaired lytic function relative to matched peripheral blood NK cells from patients with GBM or healthy donors. We attributed this immune evasion tactic to direct cell-to-cell contact between GSCs and NK cells via αv integrin–mediated TGF-β activation. Treatment of GSC-engrafted mice with allogeneic NK cells in combination with inhibitors of integrin or TGF-β signaling or with *TGFBR2* gene–edited allogeneic NK cells prevented GSC-induced NK cell dysfunction and tumor growth. These findings reveal an important mechanism of NK cell immune evasion by GSCs and suggest the αv integrin/TGF-β axis as a potentially useful therapeutic target in GBM.

Introduction

Glioblastoma multiforme (GBM), or grade IV astrocytoma, is the most common and aggressive type of primary brain tumor in adults. Despite current treatment with resection, radiotherapy, and temozolomide, the outcome for this tumor is poor, with a reported median survival of 14.6 months and a 2-year survival of 26.5%, as the tumor invariably relapses (1). This dismal outcome has stimulated keen interest in immunotherapy as a means to circumvent one or more of the factors that have limited the impact of available treatments: (a) the rapid growth rate of these aggressive tumors, (b) their molecular heterogeneity and propensity to invade critical brain structures, and (c) the tumor regenerative power of a small subset of glioblastoma stem cells (GSCs) (2, 3).

Emerging results from preclinical studies support the concept that not only mature GBM cells can be efficiently targeted by natural killer (NK) cells (4–8) but that their associated stem cells may also be highly susceptible to NK cell–mediated immune attack (9, 10). These innate-immunity lymphocytes have a broad role in protecting against tumor initiation and metastasis in many types of cancer, and they have distinct advantages over T cells as candidates for therapeutic manipulation (11, 12). However, the vast majority of tumor cells that have been studied to date possess formidable immune defenses, allowing them to evade NK cell–mediated cytotoxicity. These include disruption of receptor-ligand interactions between NK and tumor cells and the release of immunosuppressive cytokines into the microenvironment, such as transforming growth factor β (TGF-β) (13–15). Even if one could shield NK cells from the evasive tactics of GBM tumors, it may not be possible to eradicate a sufficient number of self-renewing GSCs to sustain complete responses. Indeed, very little is known about the susceptibility of GSCs to NK cell surveillance in vivo. Thus, to determine if GSCs can be targeted by NK cells in vivo, we designed a preclinical study and used single-cell analysis of primary GBM tissue from patients undergoing surgery to determine the extent to which NK cells infiltrate sites of active tumors and the potency with which they eliminate patient-derived GSCs.

Authorship note: HS, MS, RB, ABH, and KR contributed equally to this work.
Conflict of interest: HS, MS, RB, EJS, and KR have filed for a patent (MDA 20-021; UTSC.P1190US.P1; "Natural killer cell immunotherapy for the treatment of glioblastoma"). KR, EJS, REC, EL, RB, MD, PPB, DM, and The University of Texas MD Anderson Cancer Center (MDACC) have an institutional financial conflict of interest with Takeda Pharmaceutical for the licensing of the technology related to CAR-NK cells. KR, EJS, RB, EL, DM, and the MDACC has an institutional financial conflict of interest with Affimed GmbH. KR participates on Scientific Advisory Boards for GemoAb, AvengeBio, Kiadis, GSK, and Bayer.
Copyright: © 2021, American Society for Clinical Investigation.
Submitted: July 9, 2020; **Accepted:** June 3, 2021; **Published:** July 15, 2021.
Reference information: *J Clin Invest*. 2021;131(14):e142116.
https://doi.org/10.1172/JCI142116.

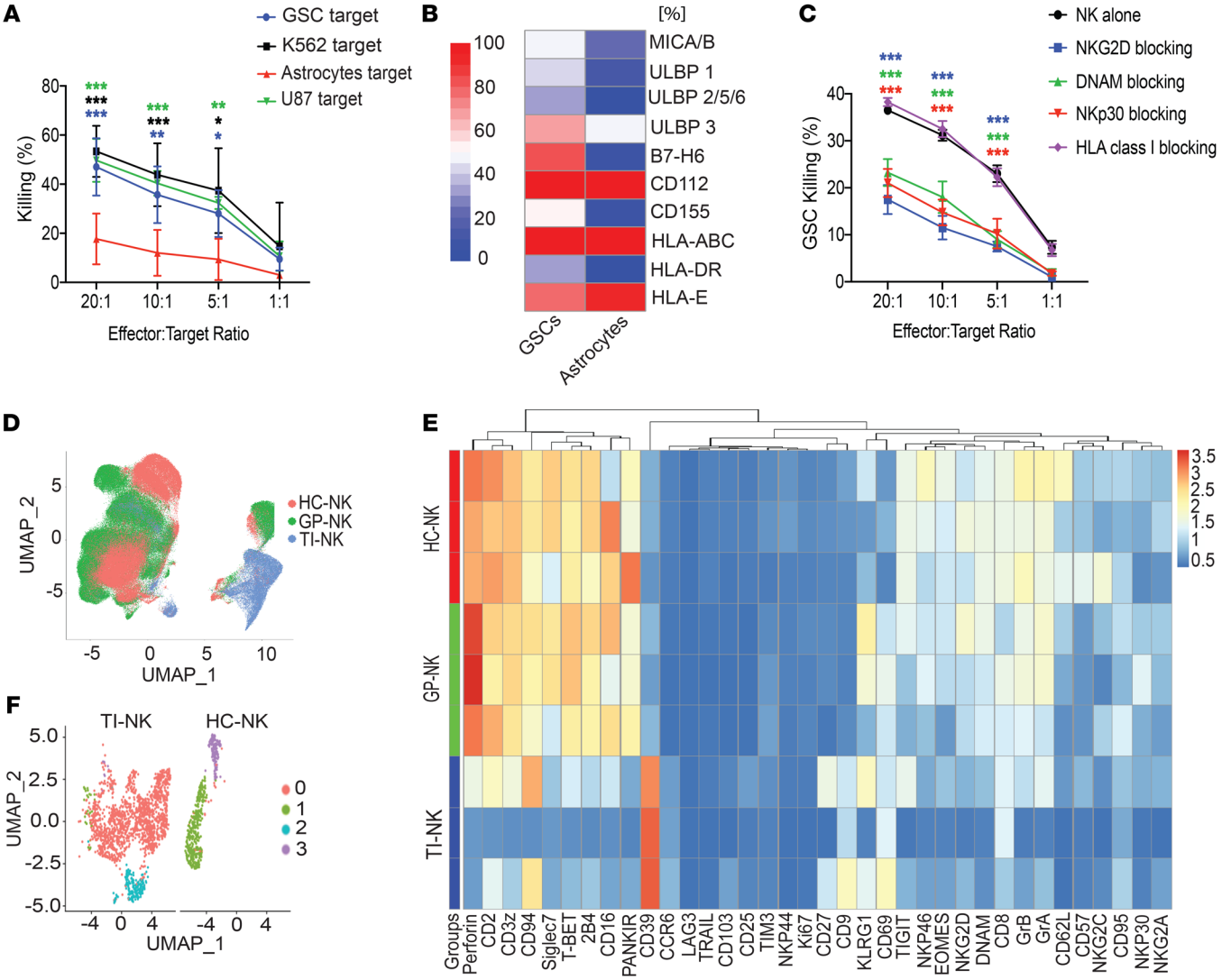
A
GSC target
K562 target
Astrocytes target
U87 target
Killing (%)
Effector:Target Ratio
20:1
10:1
5:1
1:1
B
[%]
MICA/B
ULBP 1
ULBP 2/5/6
ULBP 3
B7-H6
CD112
CD155
HLA-ABC
HLA-DR
HLA-E
GSCs
Astrocytes
C
NK alone
NKG2D blocking
DNAM blocking
NKp30 blocking
HLA class I blocking
GSC Killing (%)
Effector:Target Ratio
D
HC-NK
GP-NK
TI-NK
UMAP_2
UMAP_1
E
HC-NK
GP-NK
TI-NK
Groups
Perforin
CD2
CD3z
CD94
Siglec7
T-BET
2B4
CD16
PANKIR
CD39
CCR6
LAG3
TRAIL
CD103
CD25
TIM3
NKP44
Ki67
CD27
CD9
KLRG1
CD69
TIGIT
NKP46
EOMES
NKG2D
DNAM
CD8
GrB
GrA
CD62L
CD57
NKG2C
CD95
NKP30
NKG2A
F
TI-NK
HC-NK
UMAP_2
UMAP_1
0
1
2
3
G
Activation Markers
NCR3 (NKp30)
GZMA
GZMB
GZMK
SELL (CD62L)
FCGR3A (CD16)
CD247 (CD3ζ)
Expression Level
NS
HC-NK
TI-NK
Inhibitory Markers
KLRD1 (CD94)
KIR2DL1
KIR2DL4
TGF-β Pathway
JUND
SMAD4
SMAD7
SMURF2

Figure 1. GSCs express NK cell receptor ligands and are susceptible to NK cell cytotoxicity. (**A**) ^{51}Cr release assay showing cytotoxicity of donor-derived NK cells activated overnight with IL-15 (5 ng/mL) against GSCs (blue), K562 cells (black), U87 cell line (green), or healthy human astrocytes (red) (U87: n = 3; K562, GSCs, astrocytes: n = 6). Error bars denote SD. Green asterisks: cytotoxicity against U87 vs. astrocytes. Black asterisks: cytotoxicity against K562 vs. astrocytes. Blue asterisks: cytotoxicity against GSCs vs. astrocytes. (**B**) Heatmap representing the relative expression of NK cell ligands on GSCs or human astrocytes ranging from blue (low) to red (high). Columns represent the median expression of each receptor (GSC: n = 6; astrocytes: n = 3). (**C**) Activated HC-NK cells were cocultured with GSCs in the presence or absence of blocking antibodies: anti-NKG2D (blue), anti-DNAM (green), anti-NKp30 (red), or anti–HLA class I (purple). ^{51}Cr release assay against GSCs was assessed (n = 4). Blue asterisks: cytotoxicity against GSCs with or without anti-NKG2D. Red asterisks: cytotoxicity against GSCs with or without anti-NKp30. Green asterisks: cytotoxicity against GSCs with or without anti-DNAM. (**D** and **E**) viSNE plots (**D**) and a comparative mass cytometry heatmap (**E**) showing the expression of NK cell markers in HC-NK (red), GP-NK (green), and TI-NK cells (blue). Column clustering was identified by FlowSOM. Each row reflects annotation of the expression level for an individual patient. Color scale ranges from blue (lower expression) to red (higher expression) (n = 3). (**F**) UMAP plot showing clusters for TI-NK versus HC-NK cells by scRNA-seq. (**G**) Violin plots showing the mRNA expression levels for individual NK cell–related genes in healthy controls (HC-NK cells; blue) and TI-NK cells (red) using scRNA-seq. Markers associated with NK cell activation and cytotoxicity, inhibition, and the TGF-β pathway are presented. Statistical analysis by 2-way ANOVA with Dunnett's correction for multiple comparisons (**A** and **C**) or unpaired t test (**G**). *$P \le 0.05$; **$P \le 0.01$; ***$P \le 0.001$.

Using an experimental approach that allowed head-to-head comparison of NK cell markers at the single-cell level in the peripheral blood and primary tumor specimens from patients with GBM, we showed that NK cells have an altered phenotype that correlates with reduced NK cell cytolytic function. GSCs, which cause most recurrences of GBM tumor after therapy, proved highly susceptible to NK cell–mediated killing in vitro, but evaded NK cell recognition via a mechanism requiring direct αv integrin–mediated cell-to-cell contact, leading to the release and activation of TGF-β by the GCSs. In a patient-derived xenograft (PDX) orthotopic mouse model of GBM, GSC-induced NK cell dysfunction was completely prevented by direct blockade of αv integrin or TGF-β or by CRISPR gene editing of the TGF-β receptor 2 (*TGFBR2*) on allogeneic NK cells, resulting in effective control of the tumor. Taken together, these data suggest that inhibition of the αv integrin/TGF-β axis could overcome a major obstacle to effective NK cell immunotherapy for GBM.

Results

GSCs are susceptible to NK cell–mediated killing. GSCs can be distinguished from their mature tumor progeny at the transcriptional, epigenetic, and metabolic levels (16, 17), raising the question of whether these cells can be recognized and killed by NK cells. We therefore asked whether patient-derived GSCs, defined as being capable of self-renewal, pluripotent differentiation, and tumorigenicity when implanted into an animal host, are susceptible to NK cell cytotoxic activity as compared with healthy human astrocytes. To answer this question, we performed a 4-hour chromium-51 (^{51}Cr) release cytotoxicity assay. GSCs were derived from patients with various GBM subtypes including mesenchymal (GSC17, GSC20, GSC267, GSC272), classical (GSC231, GSC6-27), and proneural (GSC8-11, GSC262), while also showing heterogeneity in the O-6-methylguanine–DNA methyltransferase (MGMT) methylation status (methylated: GSC231, GSC8-11, GSC267, GSC272; indeterminate: GSC6-27, GSC17, GSC262). The complete transcriptional profile for each GSC is summarized in Supplemental Figure 1 (supplemental material available online with this article; https://doi.org/10.1172/JCI142116DS1). K562 cell targets were used as a positive control because of their marked sensitivity to NK cell–mediated killing due to the lack of expression of HLA class I (18). Across all effector-to-target (E:T) ratios, healthy donor NK cells killed GSCs (n = 6) and K562 cells with equal efficiency and much more readily than healthy human astrocytes (n = 6), which displayed a relative resistance to NK cell–mediated killing (Figure 1A). NK cells also efficiently targeted non-GSC glioma cell lines such as U87 (Figure 1A). Multiparametric flow cytometry was then used to analyze the expression of NK cell–activating or –inhibiting receptor ligands on GSCs. GSCs (n = 6) expressed normal levels of HLA class I and HLA-E (both ligands for inhibitory NK receptors), at levels similar to those observed on healthy human astrocytes (n = 3; Figure 1B and Supplemental Figure 2, A–C). In contrast, the ligands for activating NK receptors, such as CD155 (ligand for DNAM1), MICA/B and ULBP1/2/3 (ligands for NKG2D), and B7-H6 (ligand for NKp30) were upregulated on GSCs but not on healthy human astrocytes (Figure 1B and Supplemental Figure 2, A–C). In addition, using single-cell RNA sequencing (scRNA-seq) data generated by Darmanis et al. (19), we found that NK cell–activating ligands are also abundantly expressed on non-GSC neoplastic cells (Supplemental Figure 2D), supporting the findings that these cells are susceptible to NK cell–mediated killing. To assess the contributions of these activating and inhibitory receptors to the NK cell–dependent cytotoxicity against GSCs, we used receptor-specific blocking antibodies to disrupt specific receptor-ligand interactions. The blockade of NKG2D, DNAM1, and NKp30, but not HLA class I, significantly decreased NK cell–mediated GSC killing (n = 4; Figure 1C). Cumulatively, these findings suggest that GSCs possess the ligands needed to stimulate NK cell activation leading to GSC elimination. Indeed, the effects we observed were entirely consistent with an extant model of tumor cell attack by NK cells, whereby inhibitory signals transmitted by killer cell immunoglobulin-like receptor (KIR)–HLA class I interactions are overcome when a threshold level of activating signals are reached, inducing recognition of stressed cells (20, 21).

NK cells infiltrate GBM tumors but display an altered phenotype and function. Preclinical findings in glioma-bearing mice indicate that NK cells can cross the blood-brain barrier to infiltrate the brain (22). However, the limited clinical studies available suggest only minimal NK cell infiltration into GBM tissue (23). As such, we next investigated whether NK cells are capable of infiltrating into GBM tumors and assessed their abundance by analyzing ex vivo–resected glioma tumor specimens collected in 21 of 46 patients with primary or recurrent GBM (Table 1), and 2 of 5 patients with low-grade gliomas (Table 2). The patient characteristics are summarized in Tables 1 and 2. Each gram of GBM contained a median of 166,666 NK cells (range 9,520–600,000; n = 21), whereas there were only 500–833 NK cells/g in low-grade gliomas (n = 2). These findings indicate that NK cells can traffic into the GBM microenvironment in numbers that appear to be much larger in high-grade

Table 1. Characteristics of patients with GBM

Patient number	Sex	Age at DOS	Histology	NK cell count/ gram tissue	*IDH1* status	*MGMT* status	*TP53* status	*EGFR* status	*PTEN* status	*ATRX* loss	Previous treatment (time from last treatment to surgery)	Assay utilization
1	M	57	pGBM	N/A	N/A	N/A	N/A	N/A	N/A	N/A	none	phenotype, functional (C + L)
2	M	46	pGBM	600,000	neg	N/A	pos	N/A	N/A	N/A	none	phenotype, functional (C + L)
3	M	54	rGBM	280,000	N/A	pos	N/A	N/A	N/A	N/A	RT + TMZ (7 weeks)	phenotype, functional (C + L)
4	M	45	pGBM	9,520	neg	N/A	pos	pos	pos	N/A	none	phenotype, functional (C)
5	M	66	pGBM	370,000	neg	pos	pos	N/A	N/A	N/A	none	phenotype, functional (C + L)
6	M	38	rGBM	N/A	pos	intermediate	pos	N/A	N/A	N/A	RT + TMZ (unknown)	phenotype, functional (C), p-Smad
7	M	32	rGBM[A]	N/A	pos	N/A	pos	N/A	N/A	N/A	Accutane, RT + TMZ (3 weeks)	phenotype, p-Smad
8	F	80	pGBM	N/A	N/A	N/A	N/A	N/A	N/A	N/A	none	phenotype, functional (C), p-Smad
9	M	62	pGBM	200,000	neg	N/A	pos	N/A	N/A	N/A	none	phenotype, functional (L), p-Smad
10	F	51	pGBM	200,000	neg	pos	pos	pos	N/A	N/A	none	phenotype, p-Smad
11	M	56	pGBM	N/A	neg	neg	pos	N/A	N/A	N/A	none	phenotype
12	F	30	rGBM	300,000	pos	pos	pos	N/A	N/A	N/A	XRT + TMZ (6 weeks)	phenotype, p-Smad
13	F	55	pGBM	N/A	neg	N/A	pos	pos	pos	N/A	none	phenotype
14	F	64	pGBM	166,666	neg	N/A	pos	N/A	pos	N/A	none	phenotype
15	M	31	pGBM	133,333	neg	pos	N/A	N/A	N/A	N/A	none	functional (L)
16	F	43	pGBM	100,000	pos	pos	pos	pos	neg	N/A	none	phenotype
17	M	60	pGBM	N/A	neg	neg	N/A	pos	pos	N/A	none	phenotype
18	M	67	pGBM	N/A	neg	neg	N/A	pos	neg	N/A	none	phenotype, functional (C), reversal
19	F	42	pGBM	N/A	neg	pos	pos	pos	N/A	N/A	none	phenotype
20	M	54	rGBM	N/A	neg	neg	pos	N/A	N/A	N/A	RT + TMZ (6 weeks)	phenotype
21	M	54	rGBM	N/A	neg	N/A	pos	pos	pos	N/A	RT + TMZ (8 weeks)	functional (C), reversal
22	M	73	pGBM	266,666	neg	pos	pos	pos	mixed	N/A	none	phenotype, reversal
23	M	56	rGBM	N/A	N/A	N/A	N/A	N/A	N/A	N/A	XRT + RT + Lomustine and Avastin (6 weeks)	p-Smad
24	F	50	pGBM	N/A	neg	N/A	N/A	N/A	N/A	N/A	none	phenotype
25	M	62	pGBM	166,666	N/A	N/A	N/A	N/A	N/A	N/A	none	reversal
26	F	60	pGBM	N/A	neg	pos	N/A	pos	neg	N/A	none	phenotype
27	F	42	pGBM	N/A	N/A	neg	pos	pos	pos	neg	none	reversal
28	M	56	pGBM	116,666	neg	neg	pos	pos	neg	neg	none	functional (C)
29	M	71	pGBM	N/A	neg	neg	pos	pos	N/A	N/A	none	functional (L)
30	M	68	rGBM	N/A	neg	neg	pos	pos	neg	neg	RT + TMZ (3 weeks)	functional (L)
31	M	71	pGBM	N/A	neg	pos	pos	pos	neg	pos	none	phenotype
32	M	50	pGBM	350,000	neg	neg	neg	N/A	neg	neg	none	phenotype
33	F	61	pGBM	250,000	neg	N/A	pos	N/A	neg	neg	none	p-Smad
34	M	42	pGBM	200,000	neg	neg	pos	neg	neg	neg	none	p-Smad
35	M	50	rGBM	40,000	neg	neg	neg	neg	N/A	neg	RT + TMZ (5.5 weeks)	phenotype, p-Smad
36	F	40	pGBM	166,666	pos	pos	pos	pos	N/A	neg	none	reversal
37	F	65	pGBM	35,000	neg	pos	pos	pos	pos	neg	none	phenotype
38	M	64	pGBM	142,857	neg	neg	pos	pos	N/A	neg	none	phenotype
39	F	31	rGBM	60,000	neg	neg	pos	neg	pos	pos	RT + TMZ (4 weeks)	phenotype
40	M	65	pGBM	N/A	neg	N/A	neg	N/A	N/A	neg	none	scRNA-seq
41	M	53	pGBM	N/A	neg	N/A	pos	N/A	N/A	neg	none	scRNA-seq
42	M	52	pGBM	N/A	neg	N/A	pos	N/A	N/A	neg	none	scRNA-seq
43	M	66	pGBM	N/A	neg	neg	pos	N/A	N/A	N/A	none	scRNA-seq
44	F	70	pGBM	N/A	neg	N/A	pos	N/A	N/A	neg	none	scRNA-seq
45	M	71	rGBM	N/A	neg	pos	N/A	pos	N/A	neg	TMZ + RT + enrolled in PVSRIPO (1.5 years)	scRNA-seq
46	M	71	rGBM	N/A	neg	neg	N/A	N/A	N/A	neg	TMZ + RT (6 weeks)	scRNA-seq

[A]Arose from low-grade glioma. *IDH1*, isocitrate dehydrogenase 1; *PTEN*, phosphatase and tensin homolog; *ATRX*, α-thalassemia/mental retardation syndrome X-linked; pos, positive; neg, negative; DOS, day of surgery; pGBM, primary GBM; rGBM, recurrent GBM; TMZ, temozolomide; XRT, photon radiotherapy; RT, radiotherapy; R, reversal of NK cell dysfunction (ex vivo expansion and culture with cytokines with or without galunisertib to assess the reversal of NK cell dysfunction); C, cytokine assay; L, NK cell–mediated lysis; scRNA-seq, single-cell RNA sequencing; PVSRIPO, recombinant nonpathogenic polio–rhinovirus chimera. N/A, data not available.

Table 2. Characteristics of patients with low-grade glioma

Patient number	Sex	Age at DOS	Histology	NK cell count/ gram tissue	*IDH1* status	*MGMT* status	*TP53* status	Previous treatment	Assay utilization
1	F	34	Low-grade oligodendroglioma	500	pos	pos	pos	none	none
2	M	27	Diffuse astrocytoma	833	neg	N/A	neg	none	none
3	M	60	Low-grade oligodendroglioma	N/A	pos	N/A	N/A	none	scRNA-seq
4	F	45	Diffuse astrocytoma	N/A	pos	pos	pos	none	scRNA-seq
5	M	39	Diffuse astrocytoma	N/A	pos	neg	pos	none	scRNA-seq

IDH1, isocitrate dehydrogenase 1; pos, positive; neg, negative; DOS, day of surgery; scRNA-seq, single-cell RNA sequencing; N/A, data not available.

gliomas. We also confirmed the presence of NK cells within the GBM immune microenvironment in patients with different tumor molecular subtypes using The Cancer Genome Atlas (TCGA) GBM data set (Supplemental Figure 3) as also reported by others (24).

To gain insights into the phenotype of the GBM tumor–infiltrating NK (TI-NK) cells, we used cytometry by time-of-flight (CyToF) and a panel of 37 antibodies against inhibitory and activating receptors, as well as differentiation, homing, and activation markers (Supplemental Table 1). We ran uniform manifold approximation and projection (UMAP), a dimensionality reduction method, on a data set from paired GBM peripheral blood (PB) NK (GP-NK) cells and TI-NK cells from patients with GBM and PB from healthy controls. Heatmap analysis was used to compare protein expression between the groups. This analysis identified 4 main clusters (Figure 1, D and E). Although GP-NK cells from patients with GBM and NK cells in PB from healthy controls (HC-NK cells) showed great phenotypic similarity, they were markedly different from TI-NK cells, with the latter characterized by increased expression of CD56 ($CD56^{bright}$), upregulation of inhibitory receptors such as KLRG-1, PD-1, and CD94 (which binds to both NKG2A and NKG2C), and significantly lower levels of activating receptors (CD16, NKG2D, NKp30, NKp46, DNAM-1, NKG2C, CD2, CD3ζ, and 2B4), transcription factors (T-bet and eomes), signal-transducing adaptor proteins (DAP10, DAP12, and SAP), and cytotoxic molecules (granzyme B and perforin), as confirmed by mass cytometry (Figure 1E and Supplemental Figure 4) and by multiparameter flow cytometry in TI-NK and GP-NK cells from 28 patients with GBM compared with 15 HC-NK cells (Supplemental Figure 5, A–C).

Next, we investigated the NK cell transcriptomic profile of TI-NK cells from 10 additional glioma patients and PB mononuclear cells (PBMCs) from healthy donors using a Drop-Seq–based scRNA-seq technology (10× Genomics STAR Methods) from a soon to be publicly available data set of $CD45^+$ glioma-infiltrating immune cells (DB Zamler, unpublished observations). We analyzed over 1,746 NK cells from each patient with GBM and over 530 cells from each healthy PBMC donor. The NK signature used to define the NK population included the markers KLRD1, NKG7, and NKTR. UMAP-based analysis revealed segregation in clusters of TI-NK and HC-NK cells (Figure 1F). There was significant downregulation of genes that encode NK cell activation markers such as *NCR3* (NKp30), *GZMA* (granzyme A), *GZMK* (granzyme K), *SELL* (CD62L), *FCGR3A* (CD16), and *CD247* (CD3Z) in TI-NK cells from patients with GBM compared with HC-NK cells (Figure 1G and Supplemental Figure 5D). Genes that encode NK cell inhibitory receptors such as *KLRD1* (CD94), *KIR2DL1*, and *KIR2DL4* were upregulated in TI-NK compared with HC-NK cells (Figure 1G and Supplemental Figure 5D). Interestingly, genes associated with the TGF-β pathway, such as *JUND*, *SMAD7*, and *SMURF2*, were also significantly upregulated in TI-NK compared with HC-NK cells (Figure 1G and Supplemental Figure 5D).

We next tested the impact of our phenotypic findings on NK cell function by isolating NK cells from the GBM tumor (TI-NK cells) or GP-NK cells from patients with GBM and from healthy donors (HC-NK cells) and testing their effector function against K562 targets. TI-NK cells failed to kill K562 cell targets as determined by ^{51}Cr release assay, had less degranulation (reduced expression of CD107a), and produced significantly lower amounts of IFN-γ and TNF-α than did GP-NK or HC-NK cells (Figure 2, A and B, and Supplemental Figure 6). Taken together, these data indicate that NK cells can indeed migrate into GBM tumors but they undergo immune alteration within the tumor microenvironment that results in marked impairment of their cytotoxic function, indicating their susceptibility to immune evasion tactics of the malignant tumor.

TGF-β1 mediates NK cell dysfunction in GBM tumors. Despite the intrinsic sensitivity of GSCs to immune attack by NK cells, our findings indicate that this sensitivity is partially lost within the tumor microenvironment, where TI-NK cells are modulated toward an inhibitory phenotype. Although there are many different mechanisms that could account for this shift in function (13), the TI-NK cell phenotypic and single-cell transcriptomic alterations were most consistent with the effects of TGF-β1, a pleiotropic cytokine that functions as an important inhibitor of the mTOR pathway (25). This notion was supported by the observation of enhanced basal levels of p-Smad2/3, the canonical TGF-β signaling pathway, in TI-NK compared with GP-NK cells from patients with GBM or HC-NK cells (Figure 2C and Supplemental Figure 7).

Given the rarity of the GSCs and their exquisite sensitivity to NK cell cytotoxicity, we reasoned that they may have evolved their own mechanisms of immune evasion in addition to the evasive tactics provided by the known immunoregulatory cells in the microenvironment (13). To pursue this hypothesis, we first tested whether GSCs can suppress the function of healthy allogeneic NK cells in vitro after coculture for 48 hours. Coincubation with normal astrocytes was used as a control. After the coculture period, the NK cells were harvested and purified by bead selection and their ability to kill GSC targets was assessed in a 4-hour ^{51}Cr release assay. While

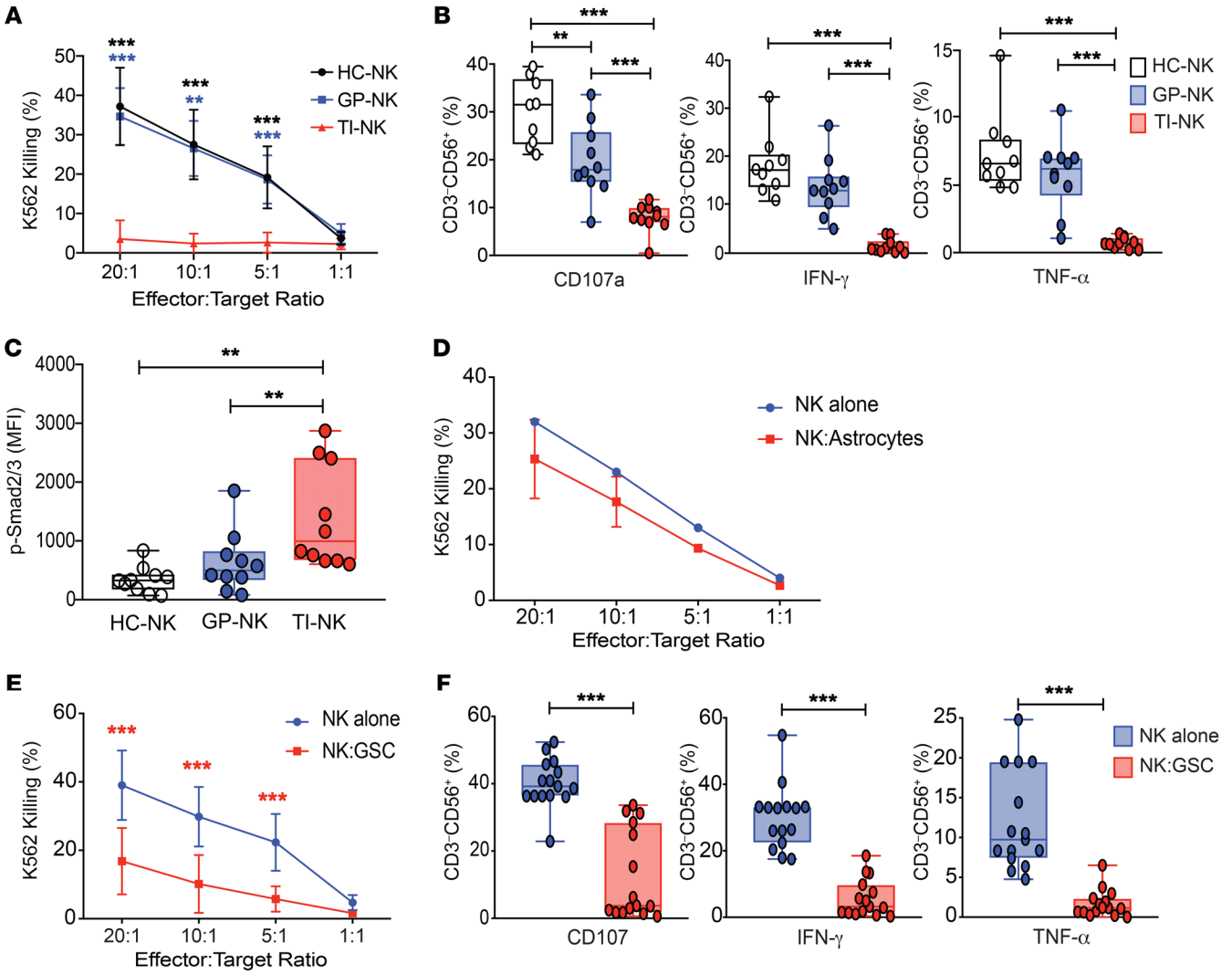

Figure 2. GSCs induce NK cell dysfunction. (**A**) Primary human GBM tumor–infiltrating NK (TI-NK) cells (red) and paired peripheral blood NK (GP-NK) cells (blue) from the same patient with GBM or peripheral blood NK cells from healthy control donors (HC-NK) (black) were cocultured for 4 hours with K562 cells at different ratios and the cytotoxicity was determined by ^{51}Cr release assay (n = 8). Black asterisks: HC-NK cell cytotoxicity against K562 targets vs. TI-NK. Blue asterisks: GP-NK cell cytotoxicity against K562 vs. paired TI-NK. (**B**) Box-and-whisker plots summarizing CD107a, IFN-γ, and TNF-α production by TI-NK, GP-NK, or HC-NK cells after incubation with K562 cells for 5 hours at a 5:1 ratio (n = 10). (**C**) Comparison of the mean fluorescence intensity (MFI) of p-Smad2/3 expression in NK cells from HC-NK (white), GP-NK (blue), and TI-NK cells (red) (n = 10). (**D**) Susceptibility of K562 to NK cells that were cocultured at a 1:1 ratio with healthy astrocytes (red) or alone (blue) for 48 hours. NK cells were then purified and their ability to kill K562 cell targets was assessed by ^{51}Cr release assay (n = 3). (**E**) Specific lysis (^{51}Cr release assay) of K562 cells by NK cells cultured alone or with GSCs at a 1:1 ratio for 48 hours (n = 10). Red asterisks: statistical significance in NK cell cytotoxicity against K562 cells for NK cells cocultured with GSCs vs. NK cells alone. (**F**) Box-and-whisker plots summarizing CD107a, IFN-γ, and TNF-α production by NK cells cultured either alone or with GSCs at a 1:1 ratio for 48 hours in response to K562 cells (n = 10). Statistical analysis by 2-way ANOVA with Dunnett's correction for multiple comparisons (**A** and **C**), 2-way ANOVA with Tukey's correction for multiple comparisons (**B**, **D**, and **E**), or paired t test (**F**). $^{**}P \le 0.01$; $^{***}P \le 0.001$.

incubation with healthy human astrocytes (control) had no effect on NK cell function (n = 3; Figure 2D and Supplemental Figure 8A), coculture with patient-derived GSCs significantly impaired the ability of allogeneic NK cells to perform natural cytotoxicity and to produce IFN-γ and TNF-α in response to K562 cell targets (n = 10 and n = 15, respectively; Figure 2, E and F, and Supplemental Figure 8B). Next, we tested whether TGF-β plays a role in GSC-induced NK cell dysfunction by coculturing NK cells from healthy control donors with patient-derived GSCs in the presence or absence of TGF-β–neutralizing antibodies and assessing their cytotoxicity against K562 cell targets. Although the antibodies did not affect the normal function of healthy NK cells when cultured alone (Supplemental Figure 9A), the blockade of TGF-β1 prevented GSCs from impairing NK cell cytotoxicity (Supplemental Figure 9, B–D). Thus, we conclude that TGF-β1 production by GSCs contributes significantly to NK cell dysfunction in the GBM microenvironment.

Disruption of TGF-β1 signaling prevents, but does not reverse, GSC-induced NK cell dysfunction. If GSCs induce NK cell dysfunction through release and extracellular activation of TGF-β1, it may be possible to avoid this evasive tactic by inhibiting the TGF-β signaling pathway. Thus, we first tested whether galunisertib (LY2157299), a TGF-β receptor I kinase inhibitor that has been used safely in patients with

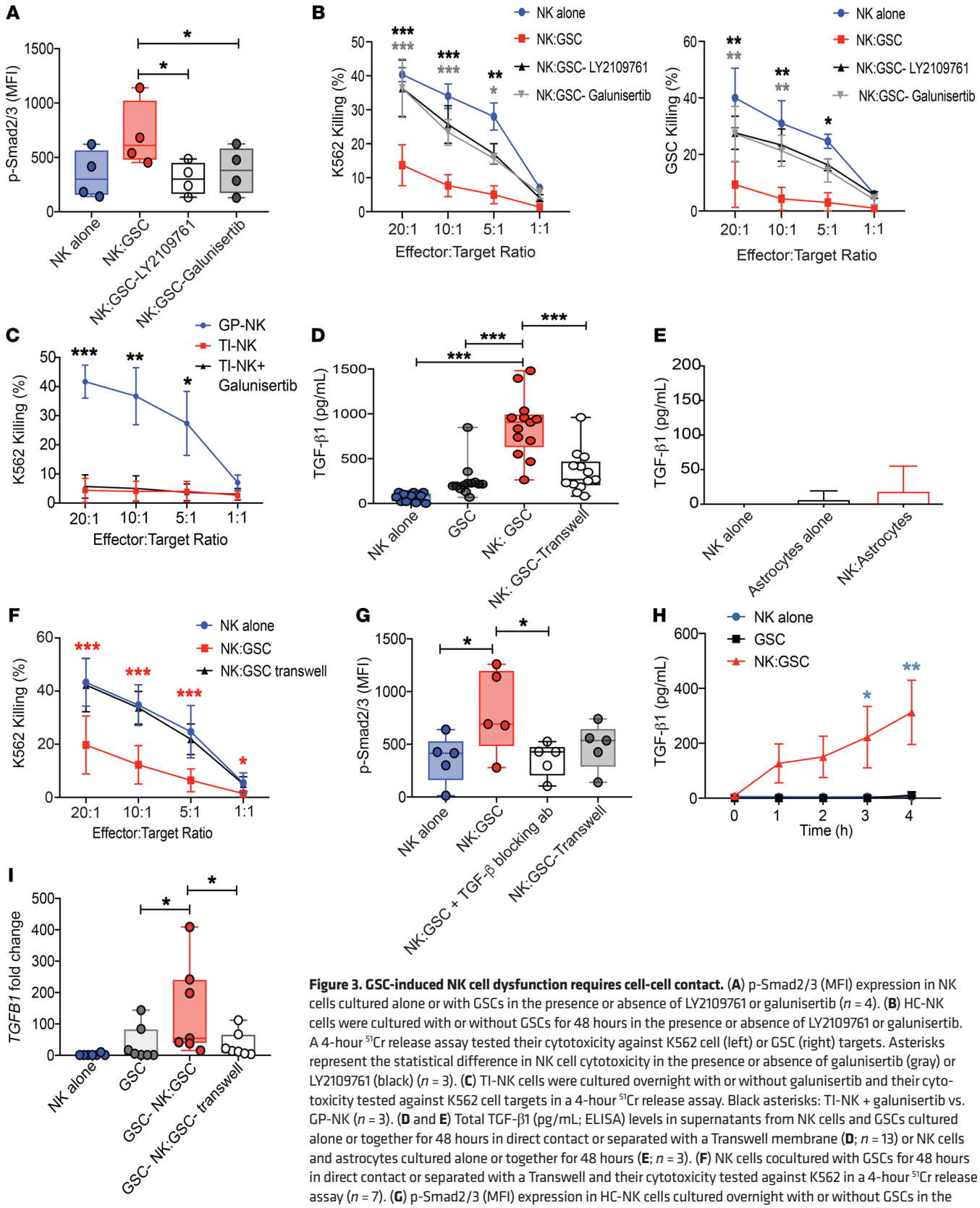

Figure 3. GSC-induced NK cell dysfunction requires cell-cell contact. (**A**) p-Smad2/3 (MFI) expression in NK cells cultured alone or with GSCs in the presence or absence of LY2109761 or galunisertib ($n = 4$). (**B**) HC-NK cells were cultured with or without GSCs for 48 hours in the presence or absence of LY2109761 or galunisertib. A 4-hour ^{51}Cr release assay tested their cytotoxicity against K562 cell (left) or GSC (right) targets. Asterisks represent the statistical difference in NK cell cytotoxicity in the presence or absence of galunisertib (gray) or LY2109761 (black) ($n = 3$). (**C**) TI-NK cells were cultured overnight with or without galunisertib and their cytotoxicity tested against K562 cell targets in a 4-hour ^{51}Cr release assay. Black asterisks: TI-NK + galunisertib vs. GP-NK ($n = 3$). (**D** and **E**) Total TGF-β1 (pg/mL; ELISA) levels in supernatants from NK cells and GSCs cultured alone or together for 48 hours in direct contact or separated with a Transwell membrane (**D**; $n = 13$) or NK cells and astrocytes cultured alone or together for 48 hours (**E**; $n = 3$). (**F**) NK cells cocultured with GSCs for 48 hours in direct contact or separated with a Transwell and their cytotoxicity tested against K562 in a 4-hour ^{51}Cr release assay ($n = 7$). (**G**) p-Smad2/3 (MFI) expression in HC-NK cells cultured overnight with or without GSCs in the presence or absence of TGF-β–blocking antibodies, or separated with a Transwell membrane ($n = 5$). (**H**) Total TGF-β1 (ELISA) in the supernatant of NK cells and GSCs cultured alone (NK: blue; GSC: black) or together (red) ($n = 4$). Blue asterisks: GSCs vs. NK:GSCs (E:T). (**I**) Fold-change in *TGFB1* mRNA levels in NK cells and GSCs cultured for 48 hours either alone, or together in direct contact or separated with a Transwell membrane ($n = 7$). Statistical analysis by 2-way ANOVA with Dunnett's (**A**–**C** and **E**–**H**), Tukey's (**D**), or Bonferroni's (**I**) correction for multiple comparisons. $^*P \le 0.05$; $^{**}P \le 0.01$; $^{***}P \le 0.001$.

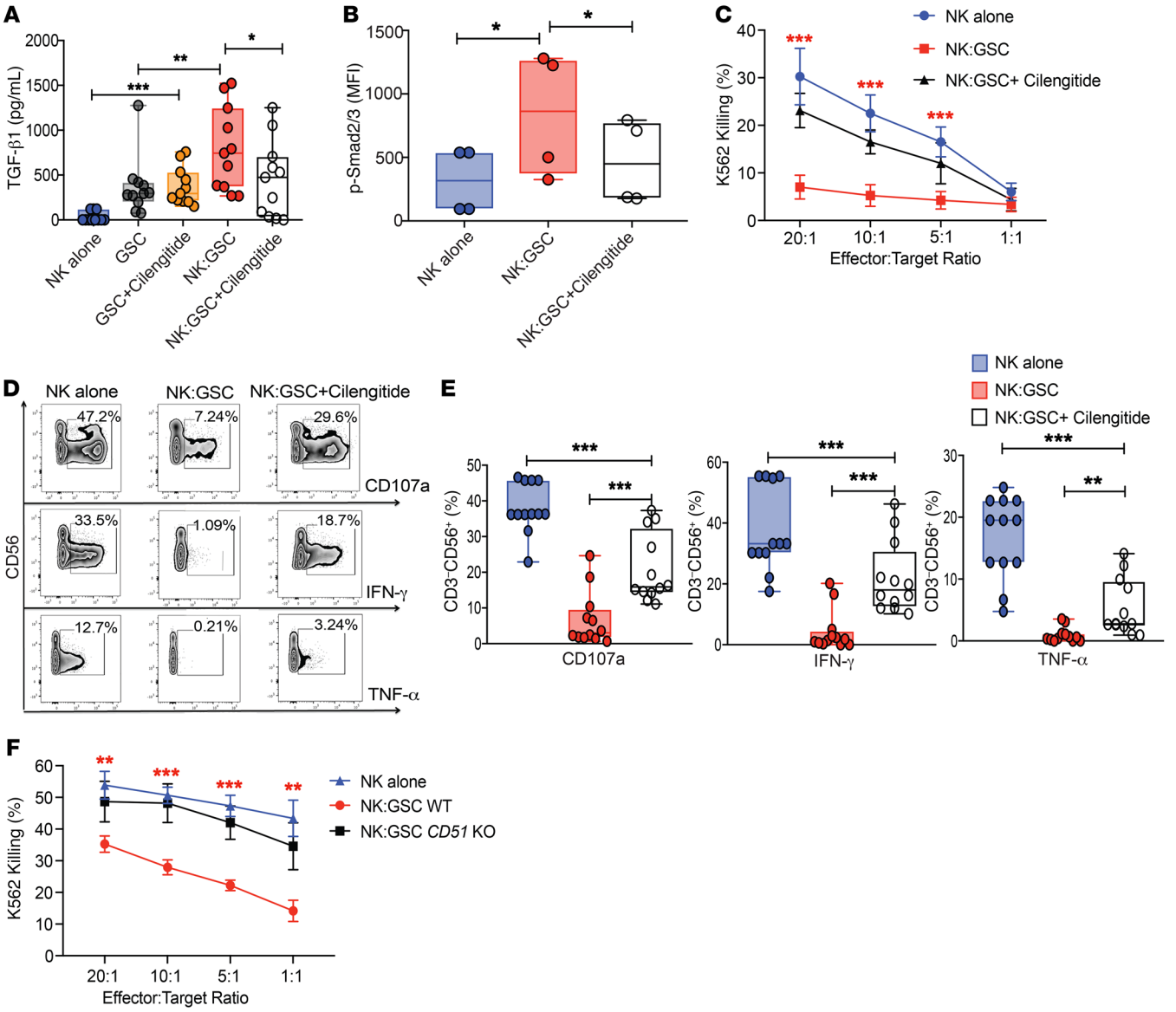

Figure 4. αv Integrins mediate TGF-β1 release by GSCs and GSC-induced NK cell dysfunction. (**A**) Box-and-whisker plots showing total TGF-β (pg/mL) in the supernatant of NK cells and GSCs cultured either alone or together in the presence or absence of the αv integrin small molecule inhibitor cilengitide (10 μM) for 48 hours was determined by ELISA ($n = 11$). (**B**) Box-and-whisker plots showing MFI of p-Smad2/3 expression on HC-NK cells cultured either alone or with GSCs in the presence or absence of cilengitide (10 μM). (**C**) ^{51}Cr release assay of K562 cell killing by NK cells cultured either alone or after coculture with GSCs for 48 hours in the presence or absence of cilengitide (10 μM) ($n = 8$). Red asterisks: specific lysis of K562 targets by NK cells that were cocultured with GSCs in the presence or absence cilengitide. (**D** and **E**) Representative zebra plots (**D**) and summary box-and-whisker plots (**E**) of CD107, IFN-γ, and TNF-α production by NK cells in response to K562 cells cultured either alone or after 48 hours of coculture with GSCs at a 1:1 ratio with or without cilengitide ($n = 12$). Inset numbers in panel **D** are the percentages of CD107a-, IFN-γ–, or TNF-α–positive NK cells within the indicated regions. (**F**) ^{51}Cr release assay of K562 cell targets by NK cells cultured either alone or with WT GSCs or with *CD51*-KO GSCs for 48 hours at a 1:1 ratio ($n = 3$). Red asterisks: the specific lysis of K562 cell targets by NK cells after coculture with WT GSCs vs. *CD51* KO. Statistical analysis by 2-way ANOVA with Bonferroni's correction for multiple comparisons (**A**, **B**, **E**, and **F**) or 2-way ANOVA with Dunnett's correction for multiple comparisons (**C**). $^*P \le 0.05$; $^{**}P \le 0.01$; $^{***}P \le 0.001$.

GBM (26), and LY2109761, a dual inhibitor of TGF-β receptors I and II (27, 28), can prevent or reverse GSC-induced NK cell dysfunction. Although neither inhibitor affected NK cell function (Supplemental Figure 10A), each prevented GSCs from activating the TGF-β1/Smad2/3 signaling pathway in NK cells (Figure 3A) and inducing dysfunction, thus preserving the natural cytotoxicity of NK cells against K562 cell or GSC targets (Figure 3B and Supplemental Figure 10, B and C). Interestingly, blockade of the TGF-β receptor kinase by galunisertib or ex vivo culture of TI-NK cells with activating cytokines such as IL-15 failed to inactivate the TGF-β1/Smad2/3 signaling pathway and restore NK cell dysfunction (Figure 3C and Supplemental Figure 10, D and E). Similarly, these conditions did not reverse the dysfunction of HC-NK cells induced by GSCs (Supplemental Figure 10, F and G), indicating that once NK cells are rendered dysfunctional in the suppressive microenvironment of GBM tumors, stimulation with IL-15 or inhibition of TGF-β1 activity is unlikely to restore their function.

GSCs induce NK cell dysfunction through cell-cell contact–dependent TGF-β release. We next asked if latent TGF-β1 complex secretion by GSCs is an endogenous process, as observed with macrophages and myeloid-derived suppressor cells (MDSCs) (29, 30), or requires active cell-cell interaction with NK cells. To address this question, we performed Transwell experiments in which healthy donor–derived NK cells and GSCs were either in direct contact with each other or separated by a 0.4 μm pore–sized permeable membrane that allowed the diffusion of soluble molecules, but not cells. Levels of total TGF-β1 were measured 48 hours after the cultures were initiated. Direct contact of GSCs with NK cells resulted in significantly higher levels of TGF-β1 compared with those attained when GSCs were separated from NK cells by a Transwell (mean 836.9 pg/mL ± 333.1 SD vs. 349 pg/mL ± 272.2 SD) or when GSCs were cultured alone (252 ± 190.4 pg/mL, $P < 0.0001$; Figure 3D), indicating that release and activation of TGF-β by GSCs is a dynamic process requiring direct cell-cell contact between the NK cells and GSCs. Importantly, healthy human astrocytes cultured either alone or with NK cells did not produce substantial amounts of TGF-β1 (Figure 3E). Consistent with these results, we found that GSC-mediated NK cell dysfunction also required direct cell-cell contact. Indeed, abrogation of direct cell-cell contact between NK cells and GSCs by a Transwell membrane prevented the induction of NK cell dysfunction and activation of the TGF-β1/Smad2/3 pathway, similar to results with TGF-β1–blocking antibodies (Figure 3, F and G, and Supplemental Figure 11).

TGF-β1 is a tripartite complex and its inactive latent form is complexed with 2 other polypeptides: latent TGF-β binding protein (LTBP) and latency-associated peptide (LAP). Activation of the mature TGF-β1 requires its dissociation from the sequestering LAP. Because TGF-β1-LAP is expressed on the surface of GSCs at high levels (Supplemental Figure 12, A and B), we asked if the increase in total TGF-β levels in the supernatant after GSC–NK cell contact was driven by release of the cytokine from the sequestering LAP or by increased transcription of the *TGFB1* gene, or both. To distinguish between these 2 alternatives, we investigated if contact with NK cells can induce a rapid release of TGF-β from LAP by measuring the kinetics of TGF-β1 production in the supernatant after GSC–NK cell coculture. The results indicate a rapid increase in total TGF-β1 levels in the supernatant as early as 1 hour after coculture in conditions where NK cells and GSCs were in direct contact compared with cocultures in which NK cells and GSCs were cultured alone (Figure 3H). When the fold-changes in *TGFB1* mRNA were determined by quantitative PCR (qPCR) in GSCs alone or in direct contact with NK cells or separated from NK cells by a Transwell membrane for 48 hours, the *TGFB1* copy numbers were significantly higher in GSCs in direct contact with NK cells ($P = 0.04$; Figure 3I). Thus, the marked increase in TGF-β1 seen after NK cell interaction with GSCs appears to involve a dual mechanism of upregulated *TGFB1* transcription and release of the mature cytokine from the LAP peptide by GSCs.

MMP2 and MMP9 play a critical role in the release of activated TGF-β1 from LAP. Both matrix metalloproteinases (MMPs) 2 and 9 mediate the release of TGF-β1 from LAP (31, 32). Because both enzymes are expressed by malignant gliomas (33), we investigated whether they might also be involved in the release of TGF-β1 from LAP and consequently in the induction of NK cell dysfunction by GSCs. First, we confirmed that GSCs are a major source of MMP2 and MMP9 (Supplemental Figure 13, A and B), and then determined their contribution to the release of TGF-β1 and GSC-induced NK cell dysfunction by culturing healthy NK cells with or without GSCs and in the presence or absence of an MMP2/9 inhibitor for 48 hours. MMPs were present at higher levels when GSCs were in direct contact with NK cells, suggesting that TGF-β1 drives their release, as confirmed by experiments using TGF-β–blocking antibodies (Supplemental Figure 13, A and B). The addition of an MMP2/9 inhibitor did not affect NK cell function in cultures lacking GSCs (Supplemental Figure 13C) but partially prevented GSC-induced NK cell dysfunction, as measured by the ability of the NK cells to perform natural cytotoxicity and to produce IFN-γ and TNF-α in response to K562 cell targets (Supplemental Figure 13, D–F). This partial restoration would be consistent with the involvement of additional pathways in the activation of TGF-β. Incubation of NK cells with the MMP2/9 inhibitor also resulted in a moderate decrease in total TGF-β and significantly lower p-Smad2/3 levels (Supplemental Figure 13, G and H), implicating MMP2/9 in the release of TGF-β by GSCs.

αv Integrins mediate cell contact–dependent TGF-β1 release by GSCs. Since GSC-mediated NK cell dysfunction requires direct cell-cell contact, we next investigated which receptor-ligand interactions could be participating in this cross-talk. Blocking the interaction of major activating and inhibitory NK cell receptors, including CD155/CD112, CD44, KIRs, and ILT-2, on healthy donor NK cells and their respective ligands on GSCs failed to prevent GSC-induced NK cell dysfunction (Supplemental Figure 14). We then changed our focus to the integrins, a family of cell surface transmembrane receptors that play a critical role not only in cell adhesion, migration, and angiogenesis, but also in the activation of latent TGF-β1 (34). The αv (CD51) integrin heterodimeric complexes αvβ3, αvβ5, and αvβ8 are highly expressed in GBM, in particular on GSCs (35). Based on evidence that targeting αv integrins in GBM can significantly decrease TGF-β production (35), we tested whether cilengitide, a small molecule inhibitor that possesses a cyclic RDG peptide with high affinity for αv integrins (αvβ3 and αvβ5) can prevent GSC-induced NK cell dysfunction by decreasing TGF-β1 production. Treatment with cilengitide significantly decreased levels of total TGF-β1 in the supernatant (Figure 4A) as well as p-Smad2/3 signaling in NK cells in direct contact with GSCs (Figure 4B) and protected NK cells from GSC-induced NK cell dysfunction ($n = 8$, $n = 12$; Figure 4, C–E). These results were confirmed by genetic silencing of the pan-αv integrin (*CD51*) in GSCs using CRISPR/Cas9 (Figure 4F and Supplemental Figure 15). Together, our data support a model in which αv integrins regulate the TGF-β1 axis involved in GSC-induced NK cell dysfunction (see graphical abstract).

We next sought to identify the surface ligands on NK cells that could potentially interact with αv integrins to mediate GSC–NK cell cross-talk. In addition to binding extracellular matrix components, αv integrins bind tetraspanins, such as CD9, through their active RDG binding site (36). Indeed, CD9 and CD103 are upregulated on GBM TI-NK cells (Supplemental Figures 4 and 5) and can be induced on healthy NK cells after coculture with TGF-β1 (Supplemental Figure 16A). Thus, we used CRISPR/Cas9 gene editing to knock out (KO) *CD9* and *CD103* in healthy donor NK cells

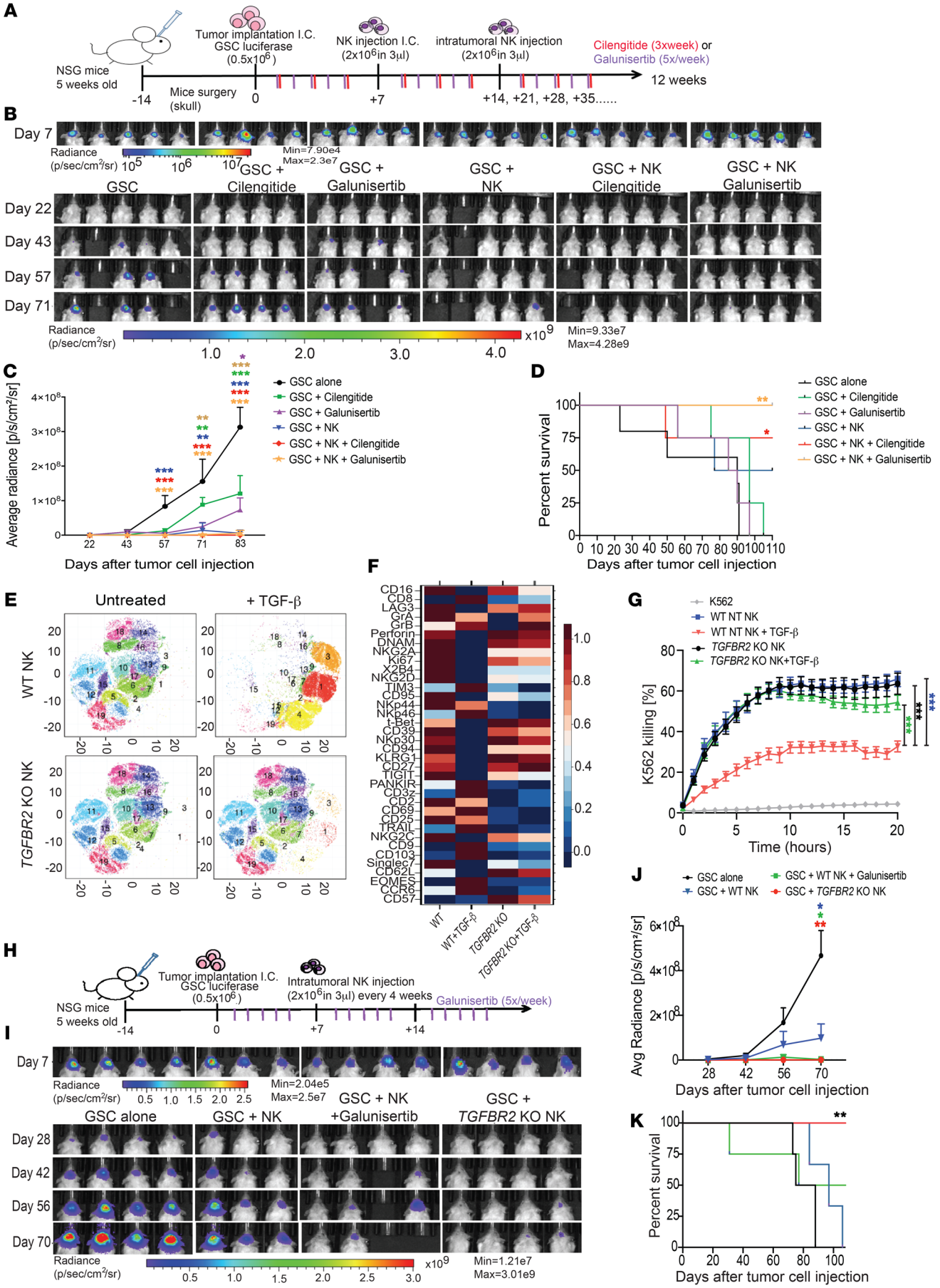
A
NSG mice
5 weeks old
Tumor implantation I.C.
GSC luciferase
(0.5x10^6)
NK injection I.C.
(2x10^6in 3µl)
intratumoral NK injection
(2x10^6in 3µl)
Cilengitide (3xweek) or
Galunisertib (5x/week)
12 weeks
Mice surgery
(skull)
-14
0
+7
+14, +21, +28, +35.....
B
Day 7
Radiance
(p/sec/cm²/sr)
Min=7.90e4
Max=2.3e7
GSC
GSC + Cilengitide
GSC + Galunisertib
GSC + NK
GSC + NK Cilengitide
GSC + NK Galunisertib
Day 22
Day 43
Day 57
Day 71
Min=9.33e7
Max=4.28e9
C
Average radiance [p/s/cm²/sr]
Days after tumor cell injection
GSC alone
GSC + Cilengitide
GSC + Galunisertib
GSC + NK
GSC + NK + Cilengitide
GSC + NK + Galunisertib
D
Percent survival
Days after tumor cell injection
E
Untreated
+ TGF-β
WT NK
TGFBR2 KO NK
F
WT
WT+TGF-β
TGFBR2 KO
TGFBR2 KO+TGF-β
G
K562
WT NT NK
WT NT NK + TGF-β
TGFBR2 KO NK
TGFBR2 KO NK+TGF-β
K562 killing [%]
Time (hours)
H
NSG mice
5 weeks old
Tumor implantation I.C.
GSC luciferase
(0.5x10^6)
Intratumoral NK injection
(2x10^6in 3µl) every 4 weeks
Galunisertib (5x/week)
I
Day 7
Min=2.04e5
Max=2.5e7
GSC alone
GSC + NK
GSC + NK +Galunisertib
GSC + TGFBR2 KO NK
Day 28
Day 42
Day 56
Day 70
Min=1.21e7
Max=3.01e9
J
GSC alone
GSC + WT NK
GSC + WT NK + Galunisertib
GSC + TGFBR2 KO NK
Avg Radiance [p/s/cm²/sr]
Days after tumor cell injection
K
Percent survival
Days after tumor cell injection

Figure 5. In vivo antitumor activity and NK cell function following TGF-β and αv integrin signaling inhibition in a GBM mouse model. (**A**) Schematic diagram showing the timeline of the in vivo experiment. (**B**) Bioluminescence imaging (BLI) at different time points was used as a surrogate marker for tumor progression (n = 4–5). (**C**) Average radiance (BLI) data. Orange asterisks: NK + galunisertib vs. tumor control. Red asterisks: NK + cilengitide vs. tumor control. Blue asterisks: NK alone vs. tumor control. Green asterisks: NK + galunisertib vs. cilengitide control. Brown asterisks: NK + cilengitide vs. cilengitide control. Purple asterisks: NK + galunisertib vs. galunisertib control. (**D**) Survival of mice in each group (n = 5). Animals treated with NK + galunisertib or NK + cilengitide had significantly better survival compared with tumor controls (P = 0.009 and P = 0.05, respectively). (**E** and **F**) viSNE plots (**E**) and comparative heatmap (**F**) of mass cytometry data showing the expression of NK cell markers in WT or *TGFBR2*-KO NK cells with or without recombinant TGF-β. Heatmap column clustering generated by FlowSOM analysis; color scale shows the expression of each marker: red (high) and blue (low). (**G**) Killing of K562 cells over time by WT-NK (blue), *TGFBR2*-KO NK (black), WT-NK + recombinant TGF-β (red), or *TGFBR2*-KO NK + recombinant TGF-β (green) as measured by real-time killing assay. (**H**) Schematic diagram showing the timeline of subsequent in vivo mouse experiment. (**I**) BLI was obtained from the 4 groups of mice (n = 4). (**J**) Average radiance (BLI) data: Red asterisks: *TGFBR2*-KO NK vs. tumor controls. Green asterisks: WT NK + galunisertib vs. tumor controls. Blue asterisks: WT NK vs. tumor controls. (**K**) Kaplan-Meier plot showing mouse survival. Statistical analysis by 2-way ANOVA with Dunnett's correction for multiple comparisons (**C**, **G**, and **J**) or log-rank test (**D** and **K**). *$P \le 0.05$; **$P \le 0.01$; ***$P \le 0.001$.

(Supplemental Figure 16B) and tested the cytotoxicity of wild-type (WT, treated with Cas9 only), *CD9*-KO, *CD103*-KO, or *CD9/CD103* double-KO NK cells after coculture with GSCs. As shown in Supplemental Figure 16, C–E, silencing of either *CD9* or *CD103* resulted in partial improvement in the cytotoxic function of NK cells cocultured with GSCs by comparison with WT control. In contrast, CD9/CD103 double-KO NK cells cocultured with GSCs retained their cytotoxicity against K562 cell targets (Supplemental Figure 16, C–E). This suggests that αv integrins on GSCs bind CD9 and CD103 on NK cells to regulate the TGF-β1 axis involved in GSC-induced NK cell dysfunction.

Inhibition of the αv integrin/TGF-β1 axis enhances NK cell antitumor activity in vivo. The mechanistic insights gained from the above studies suggest that the αv integrin/TGF-β1 axis regulates an important evasion tactic used by GSCs to suppress NK cell cytotoxic activity and therefore may provide a useful target for immunotherapy of high-grade GBM. To test this prediction, we used 2 PDX mouse models of patient-derived GSC, in which ffLuc$^+$ patient-derived GSCs (0.5×10^6 of GSC20 or GSC272) were stereotactically implanted on day 0 through a guide screw into the right forebrain of NOD/SCID/IL2Rγc-null (NSG) mice (n = 4–5 per group) and the αv integrin/TGF-β1 axis was interrupted using an αv integrin inhibitor, a TGF-β receptor kinase inhibitor, or by genetic disruption of *TGFBR2* using CRISPR/Cas9 gene editing (Figure 5 and Supplemental Figure 17). The GSC-derived PDX mouse models were confirmed to be invasive (Supplemental Figure 18), as previously reported by Sadahiro et al. (37). We first tested whether the combination of NK cells with either galunisertib to block the TGF-β signaling or cilengitide to block the integrin pathway improves the antitumor response. Seven days after tumor implantation, the mice were treated intratumorally with 2.0×10^6 human NK cells every 7 days for 11 weeks (Figure 5A). Galunisertib was administered 5 times a week by oral gavage and cilengitide 3 times a week by intraperitoneal injection. Animals implanted with tumor that were either untreated or received NK cells alone, galunisertib alone, or cilengitide alone served as controls.

As shown in Figure 5B and Supplemental Figure 17A, tumor bioluminescence, used as a surrogate to assess tumor progression, rapidly increased in untreated mice and in mice that were treated with the monotherapy cilengitide or galunisertib. By contrast, weekly administration of NK cells either alone ($P < 0.0001$) or combined with cilengitide or galunisertib (both $P < 0.0001$) led to significant improvements in tumor control compared with untreated controls (Figure 5, B and C, and Supplemental Figure 17, A and B). The best overall survival was observed when mice received NK cells combined with galunisertib (P = 0.009) or with cilengitide (P = 0.05) compared with untreated controls (Figure 5D). Similar results were also noted with the more aggressive GSC272 mouse model (Supplemental Figure 17). Immunohistochemical staining of brain specimens harvested from the animals confirmed infiltration by NK cells and direct cell-cell contact with GSCs (Supplemental Figure 19). Moreover, no evidence of tissue damage or meningoencephalitis was noted in mice treated with human allogeneic NK cells plus cilengitide or galunisertib (Supplemental Figure 20). In animals that received adoptive NK cell infusion combined with cilengitide, TI-NK cells harvested after mice were sacrificed showed a higher expression of NKG2D and reduced levels of CD9 and CD103; in contrast, NK cells harvested from animals treated with NK cells alone had a dysfunctional phenotype with lower expression of markers related to effector function (CD107a and perforin; Supplemental Figure 21). Since weekly administration of NK cells is very invasive, we explored a longer-term approach to protecting NK cells from GSC-induced NK cell dysfunction by testing the impact of *TGFBR2* KO (Supplemental Figure 22). As shown in Figure 5F, in vitro culture of WT NK cells for 48 hours with recombinant TGF-β (10 ng/mL) resulted in downregulation of activating receptors and co-receptors (CD16, NKG2D, NKG2C, DNAM, NKp30, CD2, and 2B4), and upregulation of inhibitory receptors (TIM3 and KIR). In contrast, *TGFBR2*-KO NK cells treated with recombinant TGF-β did not show significant changes in their phenotype (Figure 5, E and F), transcriptomic profile (Supplemental Figure 23, A–C), or cytotoxicity against K562 cell targets (Figure 5G and Supplemental Figure 23D). Next, we analyzed the in vivo antitumor activity of *TGFBR2*-KO NK cells by treating mice intracranially on day 7 after tumor implantation with WT NK cells, WT NK cells plus galunisertib, or *TGFBR2*-KO NK cells followed by subsequent NK cell injections every 4 weeks through a guide screw (Figure 5H). In this model, NK cells were administered less frequently (every 4 weeks) as a less invasive and more clinically translational approach. Tumor bioluminescence increased rapidly in untreated mice (GSC alone), while adoptive transfer of WT NK cells in combination with 5 times per week galunisertib or *TGFBR2*-KO NK cells led to significant tumor control as measured by bioluminescence imaging (Figure 5, I and J). However, only treatment with *TGFBR2*-KO NK cells resulted in a significant improvement in the overall survival of the animals when compared with either untreated controls (P = 0.009) or animals treated with WT NK cells (P = 0.01; Figure 5K). Treatment of NK cells alone or NK cells in combination with 5-times-per-week galunisertib every 4

weeks failed to result in a significant increase in the survival of the animals when compared with untreated controls (Figure 5K). In conclusion, our data support a combinatorial approach of NK cell adoptive therapy together with disruption of the αv integrin/TGF-β1 axis to target GBM.

Discussion

GBM is among the most deadly and most difficult to treat of all human cancers. This difficulty can be in part attributed to the presence of GSCs that differ from their mature progeny in numerous ways, including resistance to standard chemotherapy and radiotherapy, and the ability to initiate tumors and mediate recurrence following treatment. Thus, unless the GSCs within the high-grade GBM tumors are eliminated, the possibility of cure is unlikely. Here, we show the critical importance of NK cells for GBM immunosurveillance, as demonstrated by the exquisite intrinsic sensitivity of GSCs to NK cell–mediated killing and the notable influx of NK cells into the GBM microenvironment. This study is notable because its findings are based largely on profiling of primary TI-NK cells at the single-cell level in tumor samples from patients with GBM, allowing a head-to-head comparison with key markers in PB and direct ex vivo functional assessment within an individual patient. Thus, such comparisons of NK cell transcriptomes in patients revealed a shift in gene-expression profiles indicative of a functional compromise, with upregulation of inhibitory molecules and downregulation of activating molecules and systematic activation of genes related to the TGF-β pathway. This finding is consistent with a recent study in which NK cells in GBM tumors displayed an inhibitory gene expression profile with hallmarks of TGF-β–mediated inhibition (38).

TGF-β is abundantly present in the GBM microenvironment and is released by the tumor as well as several other cell types, such as regulatory T cells, M2 macrophages, and MDSCs (29, 30, 38–42). Although this cytokine is a well-characterized potent suppressor of NK cell functions (43), its mechanism of release and its contribution to GSC-induced NK cell dysfunction have remained unclear. Our working hypothesis of how GSCs evade NK cell recognition is summarized in the graphical abstract. We propose that disruption of the blood-brain barrier caused by the tumor allows NK cells to migrate into the GBM tumor tissue where they interact with GSCs, inducing both the release and the production of TGF-β by GSCs in a cell-cell contact–dependent manner that requires interaction between αv integrins on GSCs and CD9 and CD103 on NK cells. TGF-β is then cleaved from its latent complex form to its biologically active form by proteases, such as MMP2 and MMP9, released mainly by GSCs. The release of these MMPs is further driven by αv integrins and by TGF-β itself, as shown by data presented here and elsewhere (44–50). TGF-β in turn irreversibly suppresses the cytotoxic function of NK cells by inducing changes in their phenotype, transcription factors, cytotoxic molecules, and chemokines.

An important aspect of our model is the cross-talk between the αv integrins on GSCs and the TGF-β–induced receptors CD9 and CD103 on NK cells, acting as the main mediators of TGF-β production and subsequent NK cell dysfunction. Indeed, TGF-β has been reported to enhance CD103 inside-out signaling, further underscoring the complex interplay between TGF-β, CD103, and CD9 (51). We confirmed that silencing the pan-αv integrin (CD51) in GSCs by CRISPR/Cas9 gene editing or pharmacologic inhibition with cilengitide prevented GSC-induced NK cell dysfunction, diminished Smad2/3 phosphorylation, and decreased TGF-β production in cocultures of GSCs and NK cells. The αv integrins have been proposed to modulate latent TGF-β activation through 2 different mechanisms: (a) an MMP-dependent mechanism based on the production of MMP2 and MMP9 by glioma cells and GSCs, but not healthy brain tissue (33), leading to proteolytic cleavage TGF-β from LAP; and (b) an MMP-independent mechanism that relies on cell traction forces (44, 47, 49, 50, 52). This duality may explain why the MMP2/9 inhibitors used in this study could only partially protect NK cells from GSC-induced dysfunction.

Although a number of small molecules that globally inhibit TGF-β are in development for patients with GBM, most have been associated with prohibitive toxicity (53). In addition, the negative clinical data with cilengitide in GBM (54) may be at least partly explained by our observation that TGF-β inhibition prevents, but does not reverse, the state of established NK cell dysfunction induced by TGF-β in the tumor microenvironment. Taken together, these data support a combinatorial approach of NK cell immunotherapy with TGF-β or αv integrin inhibitors such as cilengitide to block TGF-β signaling by GSCs. Alternatively, gene editing strategies to delete *TGFBR2* in NK cells could be used to protect against TGF-β binding and consequent immunosuppression. With either of these strategies, it should be possible to target local immunosuppressive mechanisms only, thus reducing the risk of excessive toxicity. It should be stressed that while both weekly administration of unmodified NK cells and NK cells plus galunisertib or cilengitide could mediate effective antitumor responses (Figure 5C and Supplemental Figure 17), when the interval of therapy was increased to every 4 weeks, the unmodified NK cells failed and only *TGFBR2*-KO NK cells were capable of controlling the tumor (Figure 5K). This observation supports our in vitro data showing that while it is expected to see some short-term antitumor activity of healthy allogeneic NK cells after adoptive transfer, when the interval of administration is increased (once every 4 weeks), unmodified NK cells lose their ability to control the tumor as they become susceptible to GSC-mediated immune evasion through the release of TGF-β. The genetically modified NK cells appear to be therapeutically superior relative to the combination of NK cells with a TGF-β receptor small molecule inhibitor, possibly because the inhibitor is subjected to pharmacokinetic and pharmacodynamic parameters that influence bioavailability in the CNS and thus efficacy in the GBM microenvironment.

Finally, on the strength of these findings, we propose to develop an immunotherapeutic strategy in which third-party NK cells derived from healthy donors are administered in combination with a pan-αv integrin inhibitor or are genetically edited to silence *TGFBR2* to protect them from immunosuppression, thus enabling them to recognize and eliminate tumor cells with stem-like properties such as GSCs.

Methods

Patients. Forty-six patients with GBM (n = 34 primary GBM; n = 12 recurrent GBM) and 5 patients with low-grade glioma (n = 2 low-grade oligodendroglioma; n = 3 diffuse astrocytoma) were recruited from The University of Texas MD Anderson Cancer Center (MDACC)

for phenotyping (n = 28), functional studies (n = 14), and scRNA-seq analysis (n = 10; Tables 1 and 2). Buffy coat from normal donors was obtained from the Gulf Coast Regional Blood Center.

Characterization of TI-NK, GP-NK, and HC-NK cells. For flow cytometry, freshly isolated TI-NK, GP-NK, and HC-NK cells were incubated for 20 minutes at room temperature with Live/Dead-Aqua (Invitrogen) and surface markers. For detection of intracellular markers, cells were fixed/permeabilized using BD FACS lysing solution and permeabilizing solution 2 according to the manufacturer's instructions (BD Biosciences) followed by intracellular staining for 30 minutes at room temperature. All data were acquired with BD Fortessa (BD Biosciences) and analyzed with FlowJo software. The gating strategy for detection of NK cells is presented in Supplemental Figure 24. Details of the antibodies used in these studies are provided in the Supplemental Methods.

Mass cytometry. The strategy for antibody conjugation is described elsewhere (55). Supplemental Table 1 shows the list of antibodies used for the characterization of NK cells in the study. See Supplemental Methods for more details.

scRNA-seq. Details of the protocol are included in the Supplemental Methods. Our data set was deposited NCBI's Gene Expression Omnibus and can be found using accession number GSE147275 (https://www.ncbi.nlm.nih.gov/geo/query/acc.cgi?acc=GSE147275).

To compare the GSC and non-GSC (well differentiated, mature GBM cells), we used previous data generated by Darmanis et al. (19). As described in that paper, we used *EGFR* and *SOX9* to first identify neoplastic GBM cells and then *SOX2*, *POU3F2*, *OLIG2*, and *SALL2* to identify GSCs, while the remaining were defined as mature cells. We obtained 53 GSC and 1,038 non-GSC events for the analysis. We compared the expression of genes for the following NK cell receptor ligands: MICA/B, ULBP1-6, B7-H6, MLL-5, vimentin, HLA-E, HLA-ABC, CD113, CD111, HLA-DR, PCNA, NID-1, HLA-G, CEACAM-1, LGALS9, CD112, CD155, BAG6/BAT3, CD48, and HLA-F, and performed an unpaired t test for statistical significance.

GSC culture. GSCs were obtained from primary human GBM samples as previously described (56, 57). The GSCs were cultured in stem cell–permissive medium (neurosphere medium): Dulbecco's Modified Eagle Medium containing 20 ng/mL epidermal growth factor and basic fibroblast growth factor (all from Sigma-Aldrich); B27 (1:50; Invitrogen); 100 units/mL penicillin and 100 mg/mL streptomycin (Thermo Fisher Scientific); and passaged every 5 to 7 days (58). All generated GSC cell lines used in this study were generated at MDACC.

Characterization of GSCs and human astrocytes. Human fetal astrocyte cell lines were purchased from Lonza (CC-2565) and Thermo Fisher Scientific (N7805100); the human GBM U87 cell line (HTB-14) and the human astroglia cell line (CRL-8621) were purchased from the American Type Culture Collection (ATCC). The cells were separated into single-cell suspensions using Accutase (Thermo Fisher Scientific) for GSCs and trypsin for the attached astrocytes. The cells were then stained for 20 minutes before washing and acquiring by flow cytometry (details of the antibodies are provided in the Supplemental Methods).

NK cell cytotoxicity assays. NK cell functional and cytotoxicity assays were measured by cytokine production, NK cell degranulation, Incucyte real-time assay, and ^{51}Cr release assay. More details of these assays are provided in the Supplemental Methods. In addition to patient-derived GSCs generated from GBM tissue specimens at our institution, K562 (ATCC CCL-243, human erythroleukemia) cells were also used as targets for killing assays.

Transwell assays. NK cells (1×10^5) were either added directly to GSCs at a ratio of 1:1 or placed in Transwell chambers (Millicell, 0.4 μm; Millipore) for 48 hours at 37°C. After 48 hours, cultured cells were harvested to measure NK cell cytotoxicity by both ^{51}Cr release assay and cytokine secretion assay.

TGF-β ELISA and MMP2/9 luminex. NK cells and GSCs were either cocultured or cultured alone for 48 hours in serum-free SCGM growth medium (CellGenix). After 48 hours, supernatants were collected and the secretion of TGF-β and MMP2/3/9 was assessed in the supernatant by TGF-β1 ELISA kit (R&D Systems) or MMP2/3/9 luminex kit (eBiosciences) as per the manufacturers' protocol. For the TGF-β1 ELISA, activation was performed with 1N HCl for 10 minutes followed by neutralization with 1.2N NaOH/0.5 M HEPES prior to sample utilization.

CRISPR gene editing of primary NK cells and GSCs. crRNAs to target *CD9*, *CD103*, and *CD51* were designed using the Integrated DNA Technologies (IDT) predesigned data set. Guides with the highest on-target score and lowest off-target effect were selected. The crRNA sequences are reported in Supplemental Table 2. For more details see Supplemental Methods.

To knockout *TGFBR2*, two sgRNAs (Supplemental Table 2) spanning regions in exon 5 were designed and ordered from IDT; 1 μg cas9 (PNA Bio) and 500 ng of each sgRNA were incubated on ice for 20 minutes. After 20 minutes, 250,000 NK cells were added and resuspended in T-buffer to a total volume of 14 μL (Neon Electroporation Kit, Invitrogen) and electroporated before transfer to culture plates with antigen-presenting cells.

Xenogeneic mouse model of GBM. To assess the antitumor effect of NK cells against GSCs in vivo, we used an NSG human xenograft model (Jackson Laboratories). We have used a patient-derived-GSC mouse model because of the GSCs' superior invasiveness and migratory ability relative to conventional glioma cell lines when implanted intracranially (37). Intracranial implantation of GSCs into male mice was performed as previously described (59). A total of 140 mice were used; 0.5×10^6 patient-derived GSC20 or GSC272 were implanted intracranially into the right frontal lobe of 5-week-old NSG mice using a guide-screw system implanted within the skull. To increase the uniformity of xenograft uptake and growth, cells were injected into 10 animals simultaneously using a multiport Microinfusion Syringe Pump (Harvard Apparatus). Animals were anesthetized with xylazine/ketamine during the procedure. For in vivo bioluminescent imaging (BLI), GSCs were engineered to express luciferase by lentivirus transduction. Kinetics of tumor growth was monitored using weekly BLI (Xenogen IVIS 200 Imaging system, Caliper Life Sciences). Signal quantitation in photons/second (p/s) was performed by determining the photon flux rate within standardized regions of interest (ROIs) using Living Image software (Caliper Life Sciences). Expanded donor PB NK cells (2×10^6 in 3 μL) (60) were injected intracranially via the guide screw on day 7 after tumor implantation, and then every 7 days for 11 weeks for GSC20 and 6 weeks for GSC272. Mice were treated with either cilengitide or galunisertib (both from MCE Med Chem Express) in the presence or absence of intracranial NK cell injection. Cytokines were not administered to the mice in vivo but rather they received multiple doses of expanded NK cells. Cilengitide was administered intraperitoneally 3 times a week starting on day 1 (250 μg/100 μL PBS), while galunisertib was administered orally (75 mg/kg) by gavage 5 days a week starting on day 1 (see Figure 5A). For GSC272, mice were treated with either cilengitide or galunisertib with or without NK cells

and with *TGFBR2*-KO NK cells. In another experiment, mice were injected intracranially via the guide screw 7 days after tumor inoculation with WT NK cells, WT NK cells plus galunisertib, or *TGFBR2*-KO NK cells followed by subsequent NK cell injections every 4 weeks as describe above. Mice that presented neurological symptoms (i.e., hydrocephalus, seizures, inactivity, and/or ataxia) or moribund were euthanized. Brain tissue was then extracted and processed for NK cell extraction.

Statistics. Statistical significance was assessed with SPSS version 26 (IBM) and Prism 9.0 software (GraphPad Software, Inc.). Means were compared using unpaired *t* test, paired *t* test, 2-way ANOVA, or repeated measure ANOVA. Dunnett's correction was used when comparing to a category of reference or control; otherwise, we used Tukey's correction. Additionally, Bonferroni's correction was used to adjust for repeated measures. For survival comparison a log-rank test was used. Graphs show the mean and standard deviation (SD). All box-and-whisker plots show the median (horizontal line within the box), the 25th and 75th percentiles (bounds of the box), and minimum and maximum values (whiskers). A *P* value of less than or equal to 0.05 was considered to indicate statistical significance. When analyzing variables with more than 2 categories, *P* values were adjusted for multiple comparisons.

Study approval. All tumor tissues that were used for the generation of GSCs were resected from patients who signed written informed consents and samples were collected in accordance with the Institutional Review Board of The University of Texas MDACC in Houston (IRB protocols LAB04-0001 and LAB03-0687). All tissue samples were deindentified. All studies were performed in accordance with the Declaration of Helsinki. All animal experiments were performed in accordance with recommendations in the NIH *Guide for the Care and Use of Laboratory Animals* (National Academies Press, 2011), and approved by the Institutional Animal Care and Use Committee (IACUC) protocol number 00001263-RN01 at MDACC in Houston.

Author contributions

HS, MS and RB performed experiments and interpreted and analyzed data. KG, YH, JG, AA, NU, SL, JJL, SA, EG, JY, NWF, LL, MK, MB, AKNC, ELE, DBZ, ALG, CMJ, LNK, and YL assisted with experiments and commented on the manuscript. KC, FW, QM, JD, YS, and VM performed statistical analyses and commented on the manuscript. KG and CK provided clinical data. MD, JW, MM, LL, MM, EJS, PPB, EL, DY, REC, MB, SM, GO, NI, ME, MK, JH, GD, and FFL provided advice on experiments and commented on the manuscript. KR and ABH designed and directed the study. HS, RB, KR, DM, MS, and LMF wrote the manuscript.

Acknowledgments

This research was generously supported in part by Ann and Clarence Cazalot, the Dr. Marnie Rose Foundation, and the University of Texas MD Anderson Cancer Center Glioblastoma Moonshot Program. This work was funded by grants from the NIH (CA120813), the Specialized Program of Research Excellence (SPORE) in Brain Cancer grant (P50CA127001), and the NCI Cancer Center Support Grant (P30CA16672), which also supports the MD Anderson Flow Cytometry and Cellular Imaging Core Facility (FCCICF) that assisted with the CyTOF studies in this project. We thank our summer students Nadia Agha (University of Houston), Cindy Saliba (University of Iowa), and Lihi Shalev (Hebrew University of Jerusalem) for their assistance with some of the experiments performed in the study.

Address correspondence to: Katayoun Rezvani, Department of Stem Cell Transplantation and Cellular Therapy, The University of Texas MD Anderson Cancer Center, Houston, Texas, USA. Email: krezvani@mdanderson.org.

1. Stupp R, et al. Radiotherapy plus concomitant and adjuvant temozolomide for glioblastoma. *N Engl J Med*. 2005;352(10):987–996.
2. Bao S, et al. Glioma stem cells promote radioresistance by preferential activation of the DNA damage response. *Nature*. 2006;444(7120):756–760.
3. Lan X, et al. Fate mapping of human glioblastoma reveals an invariant stem cell hierarchy. *Nature*. 2017;549(7671):227–232.
4. Guo M, et al. Cytotoxic activity of allogeneic natural killer cells on U251 glioma cells in vitro. *Mol Med Rep*. 2016;14(1):583–589.
5. Jung TY, et al. Immunological characterization of glioblastoma cells for immunotherapy. *Anticancer Res*. 2013;33(6):2525–2533.
6. Kang SG, et al. Lymphokine activated killer cells from umbilical cord blood show higher antitumor effect against anaplastic astrocytoma cell line (U87) and medulloblastoma cell line (TE671) than lymphokine activated killer cells from peripheral blood. *Childs Nerv Syst*. 2004;20(3):154–162.
7. Kondo S, et al. Tumour necrosis factor-alpha induces an increase in susceptibility of human glioblastoma U87-MG cells to natural killer cell-mediated lysis. *Br J Cancer*. 1994;69(4):627–632.
8. Tanaka Y, et al. Ex vivo-expanded highly purified natural killer cells in combination with temozolomide induce antitumor effects in human glioblastoma cells in vitro. *PLoS One*. 2019;14(3):e0212455.
9. Weiss T, et al. NKG2D-Based CAR T cells and radiotherapy exert synergistic efficacy in glioblastoma. *Cancer Res*. 2018;78(4):1031–1043.
10. Castriconi R, et al. NK cells recognize and kill human glioblastoma cells with stem cell-like properties. *J Immunol*. 2009;182(6):3530–3539.
11. Daher M, Rezvani K. Next generation natural killer cells for cancer immunotherapy: the promise of genetic engineering. *Curr Opin Immunol*. 2018;51:146–153.
12. Rezvani K, Rouce RH. The application of natural killer cell immunotherapy for the treatment of cancer. *Front Immunol*. 2015;6:578.
13. Nduom EK, et al. Immunosuppressive mechanisms in glioblastoma. *Neuro Oncol*. 2015;17(suppl 7):9–14.
14. Gieryng A, et al. Immune microenvironment of gliomas. *Lab Invest*. 2017;97(5):498–518.
15. Beier CP, et al. The cancer stem cell subtype determines immune infiltration of glioblastoma. *Stem Cells Dev*. 2012;21(15):2753–2761.
16. Lottaz C, et al. Transcriptional profiles of $CD133^+$ and $CD133^-$ glioblastoma-derived cancer stem cell lines suggest different cells of origin. *Cancer Res*. 2010;70(5):2030–2040.
17. Shibao S, et al. Metabolic heterogeneity and plasticity of glioma stem cells in a mouse glioblastoma model. *Neuro Oncol*. 2018;20(3):343–354.
18. Nishimura M, et al. Protection against natural killer cells by interferon-gamma treatment of K562 cells cannot be explained by augmented major histocompatibility complex class I expression. *Immunology*. 1994;83(1):75–80.
19. Darmanis S, et al. Single-cell RNA-Seq analysis of infiltrating neoplastic cells at the migrating front of human glioblastoma. *Cell Rep*. 2017;21(5):1399–1410.
20. Cerwenka A, et al. Ectopic expression of retinoic acid early inducible-1 gene (RAE-1) permits natural killer cell-mediated rejection of a MHC class I-bearing tumor in vivo. *Proc Natl Acad Sci U S A*. 2001;98(20):11521–11526.
21. Zhang H, et al. Activating signals dominate inhibitory signals in CD137L/IL-15 activated natural killer cells. *J Immunother*. 2011;34(2):187–195.
22. Tran Thang NN, et al. Immune infiltration of spontaneous mouse astrocytomas is dominated by immunosuppressive cells from early stages of tumor development. *Cancer Res*. 2010;70(12):4829–4839.
23. Kmiecik J, et al. Elevated $CD3^+$ and $CD8^+$ tumor-infiltrating immune cells correlate with prolonged survival in glioblastoma patients despite integrated immunosuppressive mechanisms in the tumor microenvironment and at the systemic level. *J Neuroimmunol*. 2013;264(1–2):71–83.

24. Zhong QY, et al. A gene expression-based study on immune cell subtypes and glioma prognosis. *BMC Cancer*. 2019;19(1):1116.
25. Viel S, et al. TGF-β inhibits the activation and functions of NK cells by repressing the mTOR pathway. *Sci Signal*. 2016;9(415):ra19.
26. Capper D, et al. Biomarker and histopathology evaluation of patients with recurrent glioblastoma treated with galunisertib, lomustine, or the combination of galunisertib and lomustine. *Int J Mol Sci*. 2017;18(5):995.
27. Brandes AA, et al. A Phase II randomized study of galunisertib monotherapy or galunisertib plus lomustine compared with lomustine monotherapy in patients with recurrent glioblastoma. *Neuro Oncol*. 2016;18(8):1146–1156.
28. Zhang M, et al. Blockade of TGF-β signaling by the TGFβR-I kinase inhibitor LY2109761 enhances radiation response and prolongs survival in glioblastoma. *Cancer Res*. 2011;71(23):7155–7167.
29. Gonzalez-Junca A, et al. Autocrine TGFβ is a survival factor for monocytes and drives immunosuppressive lineage commitment. *Cancer Immunol Res*. 2019;7(2):306–320.
30. Liu Z, et al. TGF-β1 secreted by M2 phenotype macrophages enhances the stemness and migration of glioma cells via the SMAD2/3 signalling pathway. *Int J Mol Med*. 2018;42(6):3395–3403.
31. Kessenbrock K, et al. Matrix metalloproteinases: regulators of the tumor microenvironment. *Cell*. 2010;141(1):52–67.
32. Gialeli C, et al. Roles of matrix metalloproteinases in cancer progression and their pharmacological targeting. *FEBS J*. 2011;278(1):16–27.
33. Wang M, et al. The expression of matrix metalloproteinase-2 and -9 in human gliomas of different pathological grades. *Brain Tumor Pathol*. 2003;20(2):65–72.
34. Mamuya FA, Duncan MK. aV integrins and TGF-β-induced EMT: a circle of regulation. *J Cell Mol Med*. 2012;16(3):445–455.
35. Roth P, et al. Integrin control of the transforming growth factor-β pathway in glioblastoma. *Brain*. 2013;136(pt 2):564–576.
36. Yu J, et al. The CD9, CD81, and CD151 EC2 domains bind to the classical RGD-binding site of integrin αvβ3. *Biochem J*. 2017;474(4):589–596.
37. Sadahiro H, et al. Pathological features of highly invasive glioma stem cells in a mouse xenograft model. *Brain Tumor Pathol*. 2014;31(2):77–84.
38. Close HJ, et al. Expression profiling of single cells and patient cohorts identifies multiple immunosuppressive pathways and an altered NK cell phenotype in glioblastoma. *Clin Exp Immunol*. 2020;200(1):33–44.
39. Tada T, et al. Detection of active form of transforming growth factor-beta in cerebrospinal fluid of patients with glioma. *Jpn J Cancer Res*. 1993;84(5):544–548.
40. Frei K, et al. Transforming growth factor-β pathway activity in glioblastoma. *Oncotarget*. 2015;6(8):5963–5977.
41. Roy LO, et al. Differential expression and clinical significance of transforming growth factor-beta isoforms in GBM tumors. *Int J Mol Sci*. 2018;19(4):E1113.
42. Wan YY, Flavell RA. 'Yin-Yang' functions of transforming growth factor-beta and T regulatory cells in immune regulation. *Immunol Rev*. 2007;220:199–213.
43. Dahmani A, Delisle JS. TGF-β in T cell biology: implications for cancer immunotherapy. *Cancers (Basel)*. 2018;10(6):194.
44. Wipff PJ, Hinz B. Integrins and the activation of latent transforming growth factor beta1 — an intimate relationship. *Eur J Cell Biol*. 2008;87(8–9):601–615.
45. Gu X, et al. Integrin alpha(v)beta6-associated ERK2 mediates MMP-9 secretion in colon cancer cells. *Br J Cancer*. 2002;87(3):348–351.
46. Thomas GJ, et al. alpha v beta 6 Integrin upregulates matrix metalloproteinase 9 and promotes migration of normal oral keratinocytes. *J Invest Dermatol*. 2001;116(6):898–904.
47. Dutta A, et al. αvβ6 integrin is required for TGFβ1-mediated matrix metalloproteinase2 expression. *Biochem J*. 2015;466(3):525–536.
48. Deryugina EI, et al. MT1-MMP initiates activation of pro-MMP-2 and integrin alphavbeta3 promotes maturation of MMP-2 in breast carcinoma cells. *Exp Cell Res*. 2001;263(2):209–223.
49. Kim ES, et al. TGF-beta-induced upregulation of MMP-2 and MMP-9 depends on p38 MAPK, but not ERK signaling in MCF10A human breast epithelial cells. *Int J Oncol*. 2004;25(5):1375–1382.
50. Hsieh HL, et al. Transforming growth factor-β1 induces matrix metalloproteinase-9 and cell migration in astrocytes: roles of ROS-dependent ERK- and JNK-NF-κB pathways. *J Neuroinflammation*. 2010;7:88.
51. Boutet M, et al. TGFβ signaling intersects with CD103 integrin signaling to promote T-lymphocyte accumulation and antitumor activity in the lung tumor microenvironment. *Cancer Res*. 2016;76(7):1757–1769.
52. Wang J, et al. General structural features that regulate integrin affinity revealed by atypical αVβ8. *Nat Commun*. 2019;10(1):5481.
53. Herbertz S, et al. Clinical development of galunisertib (LY2157299 monohydrate), a small molecule inhibitor of transforming growth factor-beta signaling pathway. *Drug Des Devel Ther*. 2015;9:4479–4499.
54. Stupp R, et al. Cilengitide combined with standard treatment for patients with newly diagnosed glioblastoma with methylated MGMT promoter (CENTRIC EORTC 26071-22072 study): a multicentre, randomised, open-label, phase 3 trial. *Lancet Oncol*. 2014;15(10):1100–1108.
55. Li L, et al. A novel immature natural killer cell subpopulation predicts relapse after cord blood transplantation. *Blood Adv*. 2019;3(23):4117–4130.
56. Jiang H, et al. Examination of the therapeutic potential of Delta-24-RGD in brain tumor stem cells: role of autophagic cell death. *J Natl Cancer Inst*. 2007;99(18):1410–1414.
57. Pollard SM, et al. Glioma stem cell lines expanded in adherent culture have tumor-specific phenotypes and are suitable for chemical and genetic screens. *Cell Stem Cell*. 2009;4(6):568–580.
58. Gabrusiewicz K, et al. Glioblastoma stem cell-derived exosomes induce M2 macrophages and PD-L1 expression on human monocytes. *Oncoimmunology*. 2018;7(4):e1412909.
59. Lal S, et al. An implantable guide-screw system for brain tumor studies in small animals. *J Neurosurg*. 2000;92(2):326–333.
60. Shah N, et al. Antigen presenting cell-mediated expansion of human umbilical cord blood yields log-scale expansion of natural killer cells with anti-myeloma activity. *PLoS One*. 2013;8(10):e76781.